Journal of Materials Chemistry

Cite this: J. Mater. Chem., 2012, 22, 11568

www.rsc.org/materials

PAPER

Enhancement of photocatalytic activity of Bi_2WO_6 hybridized with graphite-like C_3N_4†

Yajun Wang,[ab] Xiaojuan Bai,[a] Chengsi Pan,[a] Jun He[b] and Yongfa Zhu*[a]

Received 28th December 2011, Accepted 3rd April 2012
DOI: 10.1039/c2jm16873a

Bi_2WO_6 photocatalyst was hybridized by graphite-like C_3N_4 *via* facile chemisorption. After hybridization with C_3N_4, the photocatalytic activity of Bi_2WO_6 was obviously enhanced. A C_3N_4/Bi_2WO_6 photocatalyst hybridized with monolayer C_3N_4 exhibited the highest photocatalytic activity which was 68.9% higher than that of pure Bi_2WO_6. The enhanced photocatalytic activity of the C_3N_4/Bi_2WO_6 photocatalysts could be attributed to the synergetic effect between C_3N_4 and Bi_2WO_6. The photogenerated holes on the valence band of Bi_2WO_6 could transfer to the highest occupied molecular orbital of C_3N_4 *via* the well developed interface, causing rapid photoinduced charge separation and enhancing the photocatalytic activity.

1. Introduction

Heterogeneous photocatalytic oxidation technologies are promising methods to deal with water pollutants.[1,2] To date, TiO_2 is still the most investigated and promising semiconductor material in photocatalytic oxidation.[3,4] However, very poor response to visible light has obstructed the application of TiO_2 photocatalysis in water treatment. To reduce this drawback, some efforts have been devoted to modifying the surface or bulk properties of TiO_2, such as doping,[5] combining TiO_2 with another semiconductor[6] and dye sensitization.[7] Though the above methods could partly enhance the visible light photocatalytic activity of TiO_2, some key problems are still unresolved. So from the viewpoint of using solar energy, it is very urgent to develop efficient visible-light-active photocatalysts.

Recently, many new visible-light-active photocatalysts have been reported, such as Bi_2WO_6,[8–10] $BiVO_4$,[11,12] $CaBi_2O_4$,[13] and $InVO_4$.[14,15] Nanosized Bi_2WO_6 is an excellent visible-light-active photocatalyst which has attracted a great deal of scientific interest.[9,10,16] The materials with delocalized conjugated π structures have been proven to efficiently arouse a rapid photoinduced charge separation and a relatively slow charge recombination in electron-transfer processes.[17] Our group has developed some efficient photocatalysts *via* conjugative π structured material hybridization, such as a C_{60}/TiO_2 photocatalyst,[18] a PANI/TiO_2 photocatalyst,[19] and a graphene-like carbon/TiO_2 photocatalyst.[20] Recently, Wang and co-workers reported that graphite-like C_3N_4 could absorb visible light to split water to generate hydrogen or oxygen in the presence of a sacrificial donor.[21] Graphite-like C_3N_4 (denoted as C_3N_4) possesses a very high thermal and chemical stability and has attracted extensive attention due to its outstanding mechanical, electrical, thermal, and optical properties.[22] Our group has already carried out research on a C_3N_4-hybridized ZnO photocatalyst fabricated by a chemisorption method.[23] After hybridization with C_3N_4, the photocatalytic activity of ZnO was greatly enhanced and the photocorrosion phenomenon was successfully suppressed. Moreover, surface coating is a promising way to fabricate functional materials.[24] The introduction of C_3N_4 into Bi_2WO_6 may cause a more effective charge separation of Bi_2WO_6. To the best of our knowledge, no report has been done on this topic. In this work, we present the first example of a C_3N_4-hybridized Bi_2WO_6 photocatalyst fabricated by a chemisorption method. Compared with pure Bi_2WO_6, C_3N_4-hybridized Bi_2WO_6 exhibited a higher photocatalytic activity and photocurrent. It is postulated that the enhanced photocatalytic activity of the C_3N_4/Bi_2WO_6 photocatalyst results from the high separation efficiency of photoinduced electron–hole pairs. The structure between Bi_2WO_6 and C_3N_4 as well as the mechanism of enhanced photocatalytic activity were systematically investigated.

2. Experimental section

2.1 Preparation of the C_3N_4/Bi_2WO_6 photocatalyst

Bi_2WO_6 nanosheets were prepared by the hydrothermal method according to the literature.[9] Melamine ($C_3H_6N_6$) was purchased from Sinopharm Chemical Reagent Corp, P.R. China. All other reagents were of analytical grade and were used without further purification. The C_3N_4 used in this study was prepared by

[a]*Department of Chemistry, Tsinghua University, Beijing, 100084, China. E-mail: zhuyf@mail.tsinghua.edu.cn; Fax: +86-10-62787601; Tel: +86-10-62787601*
[b]*National Center for Nanoscience and Technology, 11 Zhongguancun Beiyitiao, Beijing 100190, China*
† Electronic supplementary information (ESI) available. See DOI: 10.1039/c2jm16873a

heating melamine to 550 °C for 2 h in N_2 atmosphere according to the literature.[21] In a typical synthesis of C_3N_4/Bi_2WO_6 photocatalysts, an appropriate amount of C_3N_4 was added into methanol and was totally dispersed by ultrasonication. The as-prepared Bi_2WO_6 powder was added into the above solution and stirred in a fume hood for 24 h. After volatilization of the methanol, opaque powder was obtained after drying at 100 °C in air. C_3N_4/Bi_2WO_6 photocatalysts with other different mass ratios from 1% to 8% were prepared according to this method. Bi_2WO_6 and C_3N_4/Bi_2WO_6 electrodes were prepared as follows: 2 mg of as-prepared photocatalyst was suspended in 2 mL ethanol to produce a slurry, which was then dip-coated onto a 2 cm × 4 cm indium–tin oxide (ITO) glass electrode. Electrodes were exposed to UV light for 12 h to eliminate ethanol and subsequently calcined at 200 °C for 30 min under N_2 flow (rate = 60 mL min^{-1}). All investigated electrodes were of similar thickness (0.8–1.0 μm).

2.2 Characterization

Morphologies and microstructures of the as-prepared photocatalysts were analyzed by transmission electron microscopy (TEM) (JEM 1010, accelerating voltage 100 kV). The high-resolution transmission electron microscopy (HRTEM) images were obtained using a Tecnai TF20 transmission electron microscope operated at an accelerating voltage of 200 kV. Fourier transform infrared (FT-IR) spectra were acquired by using a Perkin Elmer System 2000 infrared spectrometer with KBr as the reference sample. X-ray photoelectron spectroscopy (XPS) was performed in a PHI 5300 ESCA system. The beam voltage was 3.0 kV, and the energy of the Ar ion beam was 1.0 keV. The binding energies were normalized to the signal for adventitious carbon at 284.8 eV. UV-vis diffuse reflectance spectra (DRS) were obtained on a UV-vis spectrophotometer (Hitachi U-3010), using $BaSO_4$ as the reference sample. The X-ray diffraction (XRD) patterns of the samples were recorded on a Bruker D8-advance diffractometer using Cu-Kα radiation (λ = 1.5418 Å). Thermogravimetric analysis (TG) and differential thermal analysis (DTA) were performed on a Dupont 1090 thermal analyzer. The atmosphere was air and the heating rate was 10 °C min^{-1}. The photoelectrochemical measurements were measured on an electrochemical system (CHI-660B, China), using a conventional three-electrode cell. Bi_2WO_6 and C_3N_4/Bi_2WO_6 electrodes served as the working electrode. The counter and the reference electrodes were a platinum wire and a saturated calomel electrode (SCE), respectively, and 0.1 M Na_2SO_4 was used as electrolyte solution. Potentials are given with reference to the SCE. The photoresponses of the photocatalysts as UV light was switched on and off were measured at 0.0 V. Electrochemical impedance spectra (EIS) were measured at 0.0 V. A sinusoidal ac perturbation of 5 mV was applied to the electrode over the frequency range of 0.05–10^5 Hz.

2.3 Photocatalytic experiments

The photocatalytic activities were evaluated by the decomposition of methylene blue (MB) under visible light and simulated solar irradiation. Visible irradiation was obtained from a 500 W xenon lamp (Institute for Electric Light Sources, Beijing) with a 450 nm cutoff filter, and the average visible light intensity was 40 mW cm^{-2}. Simulated solar irradiation was obtained from the xenon lamp without the cutoff filter. 25 mg of photocatalyst was totally dispersed in an aqueous solution of MB (100 mL, 10^{-5} mol L^{-1}). Before irradiation, the suspensions were magnetically stirred in the dark for 30 min to get an absorption–desorption equilibrium between the photocatalyst and MB. At certain time intervals, 5 mL aliquots were sampled and centrifuged to remove the particles. The concentration of MB was analyzed by recording the absorbance at the characteristic band of 633 nm using a Hitachi U-3010 UV-Vis spectrophotometer. The oxidative species in the photocatalytic system could be detected through the trapping experiments of hydroxyl radicals by using *tert*-butyl alcohol (*t*BuOH, hydroxyl radical scavenger).

3. Results and discussion

3.1 Enhancement of photocatalytic activity and photocurrent

The degradation of MB (λ > 450 nm) were carried out to investigate the photocatalytic performances of Bi_2WO_6 before and after C_3N_4 hybridization. The photocatalytic degradation of organic pollutants follows pseudo-first-order kinetics, and the values of apparent reaction rate constants k were calculated and are shown in Fig. 1a. Compared with pure Bi_2WO_6, all C_3N_4/Bi_2WO_6 photocatalysts had enhanced photocatalytic activity. When the proportion of C_3N_4 reached 2%, the C_3N_4/Bi_2WO_6 photocatalyst exhibited the optimum photocatalytic activity. The apparent rate constant k was 0.1522 h^{-1}, which was 68.9% higher than that of pure Bi_2WO_6 (0.0901 h^{-1}). When the loading amount of C_3N_4 was higher than 2%, the degradation rate decreased gradually though it remained higher than that of pure Bi_2WO_6. The loading amount of C_3N_4 had a great influence on the photocatalytic activity of the C_3N_4/Bi_2WO_6 photocatalysts. The optimal C_3N_4 loading amount of C_3N_4/Bi_2WO_6 was 2%. Moreover, pure Bi_2WO_6 and mechanically blended C_3N_4 and Bi_2WO_6 (2%) were used as references. Compared with pure Bi_2WO_6, the photocatalytic activity of mechanically blended C_3N_4 and Bi_2WO_6 (2%) was not increased. These results indicated that there may be some interaction between C_3N_4 and Bi_2WO_6 which may be of significance to enhance the photocatalytic activity.

The photocatalytic activity of C_3N_4/Bi_2WO_6-2%, C_3N_4 and Bi_2WO_6 under simulated solar irradiation was also studied (Fig. 1b), a xenon lamp was used to simulate the solar irradiation. As can be seen from Fig. 1b, the apparent rate constant k of C_3N_4/Bi_2WO_6-2% was 1.0291 h^{-1}, which was 69.8% higher than that of pure Bi_2WO_6 (0.6060 h^{-1}). The C_3N_4 hybridization can effectively enhance the photocatalytic performance of Bi_2WO_6 under simulated solar irradiation, which was similar to the result under visible light irradiation (λ > 450 nm).

The photoresponses of C_3N_4/Bi_2WO_6-2%, C_3N_4 and Bi_2WO_6 electrodes were studied and the results are shown in Fig. 2. Fast and uniform photocurrent responses of C_3N_4/Bi_2WO_6-2%, C_3N_4 and Bi_2WO_6 electrodes can be observed in Fig. 2. After hybridization with C_3N_4, the photocurrent of Bi_2WO_6 was enhanced by 2 times under visible light irradiation. The photocurrent enhancement of C_3N_4/Bi_2WO_6 originated from an enhanced photoinduced charge separation.

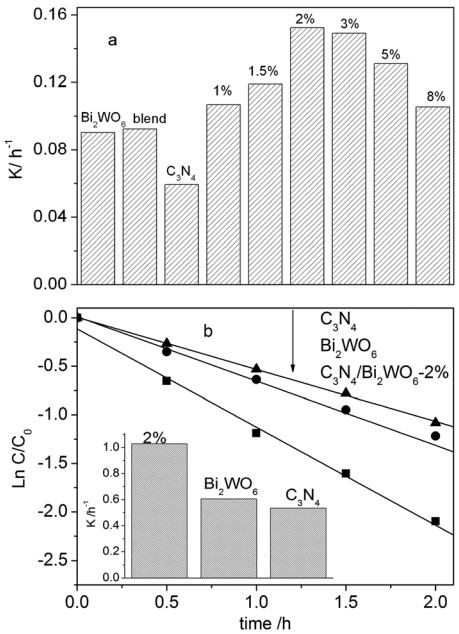

Fig. 1 Photocatalytic degradation of MB over Bi_2WO_6, C_3N_4 and C_3N_4/Bi_2WO_6 photocatalysts: (a) visible light irradiation ($\lambda > 450$ nm); (b) under xenon lamp irradiation ($\lambda > 290$ nm, simulated solar irradiation).

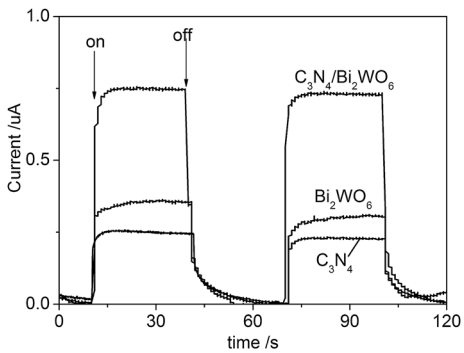

Fig. 2 Photoresponses of C_3N_4, C_3N_4/Bi_2WO_6-2% and Bi_2WO_6 electrodes ($\lambda > 450$ nm).

3.2 Structure and morphology of C_3N_4/Bi_2WO_6 photocatalysts

Fig. 3 showed the TEM and HRTEM images of Bi_2WO_6 and various C_3N_4/Bi_2WO_6 photocatalysts. As can be seen from Fig. 3(a), the Bi_2WO_6 crystals prepared by the hydrothermal process are sheet-shaped and the average size of a Bi_2WO_6 nanosheet was about 60 nm. Fig. 3(b) shows the TEM image of C_3N_4/Bi_2WO_6 photocatalyst, the Bi_2WO_6 nanosheets were surrounded by C_3N_4 shells. Fig. 3(c) shows the HRTEM image of C_3N_4/Bi_2WO_6-2% photocatalyst, there was no change of lattice structure of Bi_2WO_6 after C_3N_4 was adsorbed on the surface and the outer boundary was obviously different from the Bi_2WO_6 core. The thickness of the C_3N_4 layer coated on the C_3N_4/Bi_2WO_6-2% sample was estimated to be 0.372 nm, which was close to the scale of monolayer C_3N_4 (about 0.325 nm).[25] Therefore, it can be estimated that the absorbed C_3N_4 layer on the surface of C_3N_4/Bi_2WO_6-2% was an approximately monolayer structure. The thickness of the C_3N_4 layer increased with

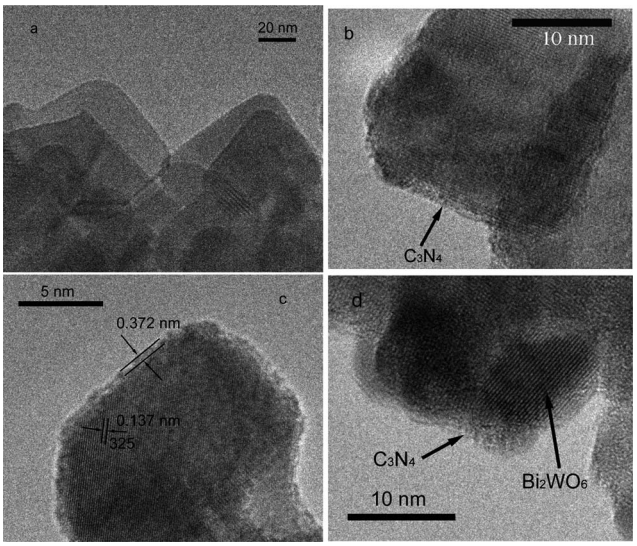

Fig. 3 TEM and HRTEM images of Bi_2WO_6 and C_3N_4/Bi_2WO_6 photocatalysts: (a) Bi_2WO_6, (b) C_3N_4/Bi_2WO_6, (c) C_3N_4/Bi_2WO_6-2%, (d) C_3N_4/Bi_2WO_6-8%.

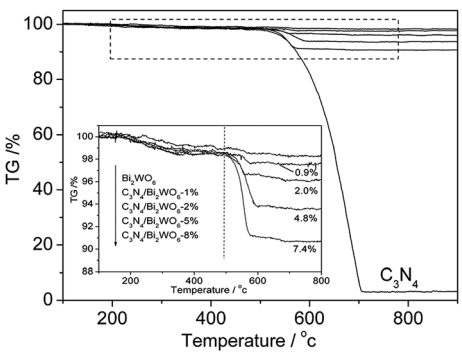

Fig. 4 TG curves of Bi_2WO_6, C_3N_4 and C_3N_4/Bi_2WO_6 photocatalysts in the presence of air. Insert: the amount of C_3N_4 hybridized on the surface of Bi_2WO_6.

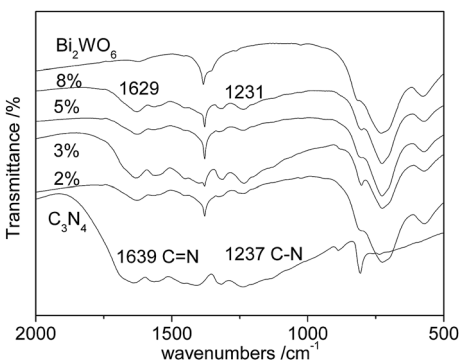

Fig. 5 FT-IR spectra of Bi_2WO_6, C_3N_4 and C_3N_4/Bi_2WO_6 photocatalysts.

increasing of the C_3N_4:Bi_2WO_6 mass ratio (Fig. 3(d)). The thickness of the C_3N_4 layer of the C_3N_4/Bi_2WO_6-8% photocatalyst was about 2 nm, indicating the C_3N_4 layer was a multilayer structure.

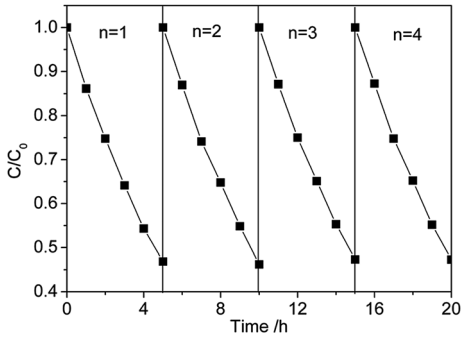

Fig. 6 Photostability experiments of C_3N_4/Bi_2WO_6 photocatalyst (MB = 10^{-5} mol L^{-1}, $\lambda > 450$ nm).

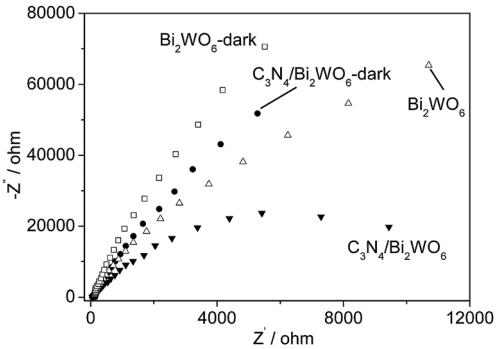

Fig. 7 EIS Nyquist plots of the Bi_2WO_6 and C_3N_4/Bi_2WO_6 photocatalysts.

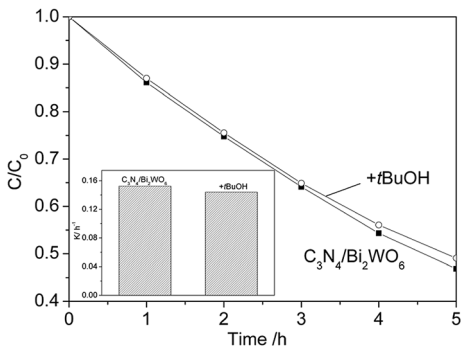

Fig. 8 The plots of photogenerated carrier trapping in the system of photodegradation of MB by C_3N_4/Bi_2WO_6 photocatalysts.

The absorption states of C_3N_4 on the surface of C_3N_4/Bi_2WO_6 could be revealed by the TG-DTA analyses (Fig. 4). As can be seen from Fig. 4, a weight loss region occurring from 200 °C to 500 °C could be observed in the TG curve of pure Bi_2WO_6, which originated from desorption of surface bound water. For pure C_3N_4, another weight loss region occurring from 500 °C to 720 °C could be found, which could be assigned to the burning of C_3N_4. These two weight loss regions could be seen in all C_3N_4/Bi_2WO_6 samples. The amount of C_3N_4 on the surface of Bi_2WO_6 could be obtained from the second weight loss, and is shown in the insert of Fig. 4. In the DTA curve of pure C_3N_4 (Fig. S1†), the endothermic peak occurring from 550 to 720 °C might be

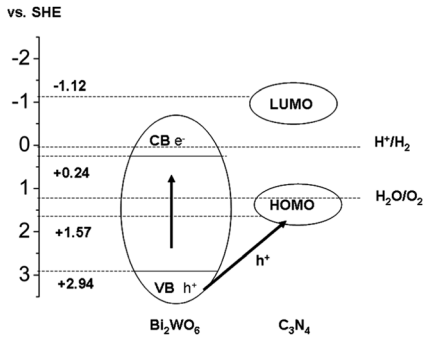

Fig. 9 Schematic drawing illustrating the mechanism of charge separation and photocatalytic activity over a C_3N_4/Bi_2WO_6 photocatalyst under irradiation.

attributed to the burning of C_3N_4. For C_3N_4/Bi_2WO_6 photocatalysts, the endothermic peak occurring from 500 to 600 °C was attributed to the burning of C_3N_4.

FT-IR spectra were determined to reveal the interface interaction between C_3N_4 and Bi_2WO_6 (Fig. 5). It could be clearly seen that the main characteristic peaks of C_3N_4 and Bi_2WO_6 all appear in the FT-IR spectra of C_3N_4/Bi_2WO_6 photocatalysts. In the FT-IR spectrum of C_3N_4, the peak at 1639 cm^{-1} and 1237 $cm^{-1}$was attributable to the C=N and C–N stretching vibrations.[26,27] Compared with that of pure C_3N_4, these main characteristic peaks all moved to lower wavenumber in the FT-IR spectra of C_3N_4/Bi_2WO_6 photocatalysts, indicating that the conjugated system of C_3N_4 was weakened and an intense interface interaction between C_3N_4 and Bi_2WO_6 occurred. To further investigate the interaction between C_3N_4 and Bi_2WO_6, XPS spectra were recorded and are shown in Fig. S2.† Compared with pure C_3N_4, the binding energy of N 1s of C_3N_4/Bi_2WO_6-2% showed a negative shift. Due to the low loading concentration of C_3N_4, the peak of N 1s of C_3N_4/Bi_2WO_6-2% was weak. In contrast, the binding energy of Bi 4f of C_3N_4/Bi_2WO_6-2% exhibited a positive shift as compared to pure Bi_2WO_6. These results showed that there was an intense interface interaction between Bi and N atoms, not a simply physical adsorption. This interaction was essential to transfer carriers and enhance photocatalytic activity.

A comparison of the UV-vis DRS spectra of Bi_2WO_6 and different mass ratios of C_3N_4/Bi_2WO_6 photocatalysts is displayed in Fig. S3.† The Bi_2WO_6 photocatalyst showed a fundamental absorption edge at 470 nm, which corresponds to the visible light photocatalytic activity. After hybridization with C_3N_4, the C_3N_4/Bi_2WO_6 photocatalysts showed the same absorption edge as Bi_2WO_6, indicating identical band gap energies. With the increasing amount of C_3N_4, the absorption intensity of C_3N_4/Bi_2WO_6 photocatalysts did not obviously change.

The XRD patterns of Bi_2WO_6, C_3N_4 and various C_3N_4/Bi_2WO_6 photocatalysts are shown in Fig. S4.† All the diffraction peaks of Bi_2WO_6 can be exactly indexed as the square Bi_2WO_6 structure (JCPDS 73-1126). The XRD patterns of Bi_2WO_6 showed no change when Bi_2WO_6 was hybridized with C_3N_4, indicating the hybridization of C_3N_4 did not influence the lattice structure of Bi_2WO_6. No XRD diffraction peaks indexed to C_3N_4 were observed because the C_3N_4 layer was too thin.

3.3 Stability of the C_3N_4/Bi_2WO_6 photocatalysts

To evaluate the stability of the as-prepared C_3N_4/Bi_2WO_6 photocatalysts, 4 recycling experiments for the photodegradation of MB were performed (Fig. 6). After being used 4 times for MB degradation, the rate constants of MB degradation of C_3N_4/Bi_2WO_6-2% declined from 0.1522 h^{-1} to 0.1501 h^{-1}. This result indicated the as-prepared C_3N_4/Bi_2WO_6 photocatalysts were photostable during the photocatalytic degradation.

3.4 Mechanism of enhancement of photocatalytic activity

Photocatalytic activity was governed by some crucial factors, such as phase structure, adsorption ability, and separation efficiency of photogenerated electrons and holes.[28] XRD patterns of C_3N_4/Bi_2WO_6 exhibited similar diffraction peaks as those of Bi_2WO_6, indicating the crystal phase structure of Bi_2WO_6 was not changed after C_3N_4 hybridization (Fig. S4†). Compared with that of pure Bi_2WO_6, C_3N_4/Bi_2WO_6 showed an enhanced adsorptivity (Fig. S5†). After adsorption equilibrium, 69.9% and 62.6% of MB remained in the solution with pure Bi_2WO_6 and C_3N_4/Bi_2WO_6-2% photocatalyst, respectively. The enhancement of adsorption could be attributed to the π–π stacking between MB and C_3N_4.[23]

The separation efficiency of photogenerated electrons and holes is a crucial factor for photocatalytic activity. The interface charge separation efficiency was investigated by EIS. Fig. 7 showed the EIS Nyquist plots of Bi_2WO_6 and C_3N_4/Bi_2WO_6 photocatalysts without and with irradiation. The radius of the arc on the EIS spectra reflects the reaction rate occurring at the surface of the electrode.[29,30] The smaller arc radius on the EIS Nyquist plot of C_3N_4/Bi_2WO_6 under irradiation indicates that a more effective separation of photogenerated electron–hole pairs and a faster interfacial charge transfer had occurred. The arc radius on the EIS Nyquist plot of C_3N_4/Bi_2WO_6 was also smaller than that of Bi_2WO_6 without irradiation, suggesting that the introduction of C_3N_4 changed the charge distribution of Bi_2WO_6 and made charge transfer easier. This result indicated that the introduction of C_3N_4 into Bi_2WO_6 can effectively enhance the separation efficiency of photogenerated electron–hole pairs.

To reveal the photocatalytic mechanism, the main oxidative species in the photocatalytic process were detected through the trapping experiments of hydroxyl radicals by using *t*BuOH (hydroxyl radical scavenger). As shown in Fig. 8, the photocatalytic activity of C_3N_4/Bi_2WO_6 was not changed by the addition of the scavenger for hydroxyl radicals, indicating that the hydroxyl radicals were not the main oxidative species of the C_3N_4/Bi_2WO_6 system. Therefore, the main oxidative species of the C_3N_4/Bi_2WO_6 system would be holes.

As discussed above, the phase structure of Bi_2WO_6 remained unchanged and the adsorptivity of Bi_2WO_6 increased a little, so we may conclude that the enhancement of the photocatalytic activity of the C_3N_4/Bi_2WO_6 photocatalysts was attributed mainly to the effective separation of the photogenerated electron–hole pairs. Fig. 9 shows the schematic for electron–hole separation and transportation at the C_3N_4/Bi_2WO_6 photocatalyst interface. The conduction band (CB) and valence band (VB) potentials of the Bi_2WO_6 are shown in Fig. 9. Bi_2WO_6 can absorb visible light to produce photogenerated electron–hole pairs. Since the VB position of Bi_2WO_6 (+2.94 eV) was lower than the highest occupied molecular orbital (HOMO) of C_3N_4 (+1.57 eV),[16,25] the photogenerated holes on Bi_2WO_6 could transfer easily to C_3N_4 *via* the well developed interface. Thus, the charge recombination could be effectively suppressed, leaving more hole charge carriers and enhancing the photocatalytic activity.

4. Conclusion

In summary, C_3N_4/Bi_2WO_6 photocatalysts were prepared *via* facile chemisorption. The photocatalytic activity of C_3N_4/Bi_2WO_6 was obviously enhanced compared to pure Bi_2WO_6. A C_3N_4/Bi_2WO_6 photocatalyst hybridized with monolayer C_3N_4 (0.372 nm) showed the highest photocatalytic activity which was 68.9% higher than that of pure Bi_2WO_6. The enhanced photocatalytic activity of the C_3N_4/Bi_2WO_6 photocatalysts could be attributed to the rapid photoinduced charge separation caused by the hybridization of C_3N_4. This work demonstrated that C_3N_4 is a very promising candidate for development of highly active photocatalysts, and C_3N_4 hybridization could be a new possibility to design new photocatalysts with high performance for environmental applications.

Acknowledgements

This work was partly supported by Chinese National Science Foundation (20925725 and 20673065) and National Basic Research Program of China (2007CB613303).

References and Notes

1 C. C. Wong and W. Chu, *Environ. Sci. Technol.*, 2003, **37**, 2310–2316.
2 A. Mills and S. Le Hunte, *J. Photochem. Photobiol., A*, 1997, **108**, 1–35.
3 K. I. Hadjiivanov and D. G. Klissurski, *Chem. Soc. Rev.*, 1996, **25**, 61.
4 A. Fujishima, T. N. Rao and D. A. Tryk, *J. Photochem. Photobiol., C*, 2000, **1**, 1–21.
5 R. Asahi, T. Morikawa, T. Ohwaki, K. Aoki and Y. Taga, *Science*, 2001, **293**, 269–271.
6 W. Chengyu, S. Huamei, T. Ying, Y. Tongsuo and Z. Guowu, *Sep. Purif. Technol.*, 2003, **32**, 357–362.
7 Y. Cho, W. Choi, C.-H. Lee, T. Hyeon and H.-I. Lee, *Environ. Sci. Technol.*, 2001, **35**, 966–970.
8 J. Tang, Z. Zou and J. Ye, *Catal. Lett.*, 2004, **92**, 53–56.
9 C. Zhang and Y. Zhu, *Chem. Mater.*, 2005, **17**, 3537–3545.
10 H. Fu, C. Pan, W. Yao and Y. Zhu, *J. Phys. Chem. B*, 2005, **109**, 22432–22439.
11 A. Kudo, K. Omori and H. Kato, *J. Am. Chem. Soc.*, 1999, **121**, 11459–11467.
12 S. Tokunaga, H. Kato and A. Kudo, *Chem. Mater.*, 2001, **13**, 4624–4628.
13 J. Tang, Z. Zou and J. Ye, *Angew. Chem., Int. Ed.*, 2004, **43**, 4463–4466.
14 J. Ye, Z. Zou, M. Oshikiri, A. Matsushita, M. Shimoda, M. Imai and T. Shishido, *Chem. Phys. Lett.*, 2002, **356**, 221–226.
15 L. Zhang, H. Fu, C. Zhang and Y. Zhu, *J. Solid State Chem.*, 2006, **179**, 804–811.
16 H. Fu, L. Zhang, W. Yao and Y. Zhu, *Appl. Catal., B*, 2006, **66**, 100–110.
17 G. Yu, J. Gao, J. C. Hummelen, F. Wudl and A. J. Heeger, *Science*, 1995, **270**, 1789–1791.
18 L. Zhang, Y. Wang, T. Xu, S. Zhu and Y. Zhu, *J. Mol. Catal. A: Chem.*, 2010, **331**, 7–14.
19 H. Zhang, R. Zong, J. Zhao and Y. Zhu, *Environ. Sci. Technol.*, 2008, **42**, 3803–3807.
20 Y. Wang, R. Shi, J. Lin and Y. Zhu, *Appl. Catal., B*, 2010, **100**, 179–183.

21 X. Wang, K. Maeda, A. Thomas, K. Takanabe, G. Xin, J. M. Carlsson, K. Domen and M. Antonietti, *Nat. Mater.*, 2009, **8**, 76–80.
22 J. m. Hu, *Appl. Phys. Lett.*, 2006, **89**, 261117.
23 Y. Wang, R. Shi, J. Lin and Y. Zhu, *Environ. Sci. Technol.*, 2011, **4**, 2922–2929.
24 W. Li, Y. Deng, Z. Wu, X. Qian, J. Yang, Y. Wang, D. Gu, F. Zhang, B. Tu and D. Zhao, *J. Am. Chem. Soc.*, 2011, **133**, 15830–15833.
25 S. C. Yan, S. B. Lv, Z. S. Li and Z. G. Zou, *Dalton Trans.*, 2010, **39**, 1488–1491.
26 Y. Zhao, D. Yu, H. Zhou, Y. Tian and O. Yanagisawa, *J. Mater. Sci.*, 2005, **40**, 2645–2647.
27 X. Li, J. Zhang, L. Shen, Y. Ma, W. Lei, Q. Cui and G. Zou, *Appl. Phys. A: Mater. Sci. Process.*, 2009, **94**, 387–392.
28 L.-W. Zhang, H.-B. Fu and Y.-F. Zhu, *Adv. Funct. Mater.*, 2008, **18**, 2180–2189.
29 W. H. Leng, Z. Zhang, J. Q. Zhang and C. N. Cao, *J. Phys. Chem. B*, 2005, **109**, 15008–15023.
30 H. Liu, S. Cheng, M. Wu, H. Wu, J. Zhang, W. Li and C. Cao, *J. Phys. Chem. A*, 2000, **104**, 7016–7020.